PNAS RESEARCH ARTICLE | APPLIED PHYSICAL SCIENCES

A spectral machine learning approach to derive central aortic pressure waveforms from a brachial cuff

Alessio Tamborini[a,1], Arian Aghilinejad[a], and Morteza Gharib[a]

Affiliations are included on p. 10.

Edited by Charles Peskin, New York University, New York, NY; received August 12, 2024; accepted January 16, 2025

Analyzing cardiac pulse waveforms offers valuable insights into heart health and cardiovascular disease risk, although obtaining the more informative measurements from the central aorta remains challenging due to their invasive nature and limited noninvasive options. To address this, we employed a laboratory-developed cuff device for high-resolution pulse waveform acquisition and constructed a spectral machine learning model to nonlinearly map the brachial wave components to the aortic site. Simultaneous invasive aortic catheter and brachial cuff waveforms were acquired in 115 subjects to evaluate the clinical performance of the developed wave-based approach. Magnitude, shape, and pulse waveform analysis on the measured and reconstructed aortic waveforms were correlated on a beat-to-beat basis. The proposed cuff-based method reconstructed aortic waveform contours with high fidelity (mean normalized-RMS error = 11.3%). Furthermore, continuous signal reconstruction captured dynamic aortic systolic blood pressure (BP) oscillations (r = 0.76, $P < 0.05$). Method-derived central pressures showed strong correlation with the independent invasive measurement for systolic BP (R^2 = 0.83; B [LOA] = −0.3 [−17.0, 16.4] mmHg) and diastolic BP (R^2 = 0.58; B [LOA] = −0.7 [−13.1, 11.6] mmHg). Shape-based features are effectively captured by the spectral machine learning method, showing strong correlations and no systemic bias for systolic pressure–time integral (r = 0.91, $P < 0.05$), diastolic pressure–time integral (r = 0.95, $P < 0.05$), and subendocardial viability ratio (r = 0.86, $P < 0.05$). These results suggest that the nonlinear transformation of wave components from the distal to the central site predicts the morphological waveform changes resulting from complex wave propagation and reflection within the cardiovascular network. The proposed wave-based approach holds promise for future applications of noninvasive devices in clinical cardiology.

central pressure waveform | transfer function | cuff-based device | machine learning | aortic catheterization

Significance

Mapping peripheral to central pressure waveforms offers a promising approach for noninvasive assessment of the aortic pressure waveform. Traditional methods rely on population-based averaging, which fail to account for the complex wave interactions within the arterial system, leading to poor morphological accuracy. This study introduces a wave-based approach that combines brachial cuff measurements with machine learning to nonlinearly map brachial wave components to the aortic site, enabling accurate reconstruction of the central pressure waveform. By accounting for nonlinear wave interactions, this method achieves higher-fidelity waveform reconstruction, improving central pulse wave analysis. Importantly, integration into clinical practice is straightforward, leveraging automated, noninvasive brachial cuff measurements already widely used in healthcare.

Cardiovascular disease (CVD) remains the leading cause of death in the United States, affecting millions of people each year (1). Early detection and accurate monitoring of heart health are crucial for preventing serious complications such as heart attack, stroke, and chronic heart failure, which have had an annual cost of around $400 billion on the US economy (1). Evaluating blood pressure (BP) is essential for assessing cardiovascular risk, as the heart works against the BP to efficiently eject blood into the arterial system (2). In clinical practice, BP is typically measured noninvasively at the brachial artery using a cuff-based device. The brachial systolic BP (SBP) and diastolic BP (DBP), representing the peak and trough of the cardiac pressure wave, serve as surrogates for central pressure due to their convenience and are widely used for initial CVD risk assessment (3). However, increasing evidence indicates that factors beyond BP play a crucial role in the development of cardiac disease and are independent risk factors (4, 5). These findings have supported a strong paradigm shift toward analyzing the entire pressure waveform shape to quantitatively assess these additional risk factors through pulse wave analysis (PWA) (6).

As the cardiac pressure wave travels from the central to peripheral arteries, its shape and amplitude are altered by the interaction between forward-propagating and reflected waves (Fig. 1*A*) (7–9). Most notably, as the pressure wave propagates distally, SBP increases while DBP and mean arterial pressure (MAP) remain relatively constant (10). These transformations are influenced by subject-specific hemodynamic factors, such as arterial stiffness and wave reflection intensity, resulting in significant variability in waveform morphology and magnitude changes between central and peripheral arteries among individuals (8, 11, 12). Evidence increasingly shows that central BP is more strongly linked to target organ damage and CVD risk than peripheral BP (12, 13). Antihypertensive drugs affect central and peripheral BP differently by targeting distinct mechanisms such as total peripheral resistance, cardiac output, arterial stiffness, and wave reflections. Since the

Author contributions: A.T., A.A., and M.G. designed research; A.T. performed research; A.T. contributed new analytic tools; A.T. analyzed data; A.A. and M.G. reviewed the data analysis; reviewed the paper; and A.T. wrote the paper.

Competing interest statement: A.T. is a consultant for Avicena LLC. M.G. is a co-founder of Avicena LLC. Through Caltech, A.T. and M.G. have a pending patent for the cuff-based device. Through Caltech, A.T., A.A., and M.G. have a pending patent for the cuff-ML method.

This article is a PNAS Direct Submission.

[1]To whom correspondence may be addressed. Email: atambori@caltech.edu.

This article contains supporting information online at https://www.pnas.org/lookup/suppl/doi:10.1073/pnas.2416006122/-/DCSupplemental.

Published February 26, 2025.

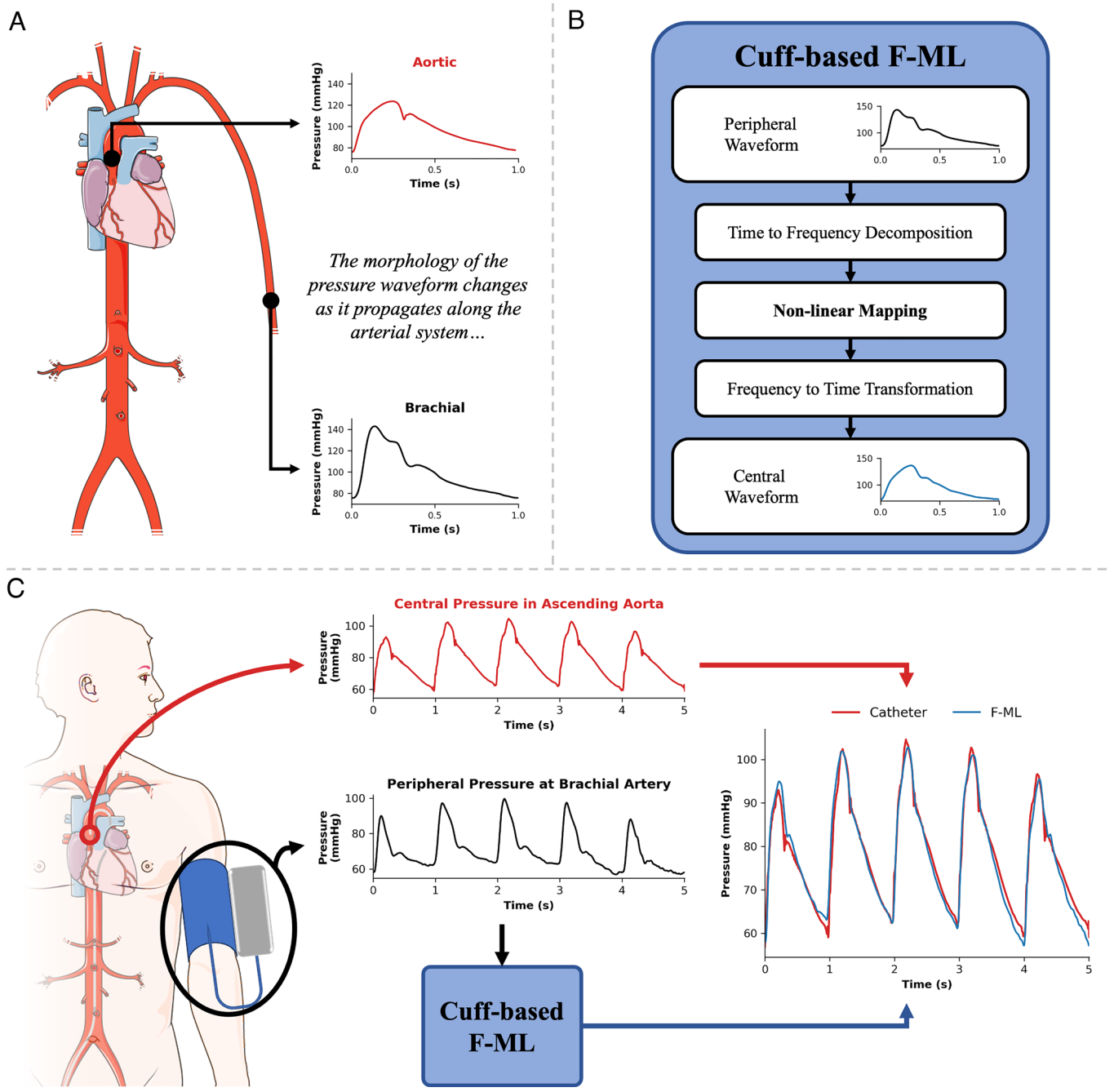

Fig. 1. Overview of the study's motivation, methodology, and design. (*A*) Real waveform examples illustrating the morphological changes that occur as pressure waves propagate through the arterial system. (*B*) Steps of the cuff-based F-ML approach for reconstructing central pressure waveforms. (*C*) Study design for the simultaneous acquisition of invasive aortic catheter waveforms and brachial cuff waveforms. F-ML was applied to calibrated peripheral waveforms obtained from the brachial cuff to reconstruct the corresponding aortic pressure waveform. Part of this figure was generated with adapted illustrations from Servier Medical Art, provided by Servier and licensed under a Creative Commons Attribution 3.0 Unported License.

causes of elevated BP vary, evaluation of treatment efficacy should extend beyond brachial BP measurements to include central pressure waveform analysis (12, 14). Given that direct measurement of the central waveform requires invasive procedures with associated risks, there arises a need for a peripheral-to-central transformation. To this end, there has been an emerging interest in developing techniques to estimate the shape of the central pressure waveform from a noninvasive peripheral measurement (15). The conventional method of estimating central pressure was achieved with the Generalized Transfer Function (GTF) (16, 17). However, it was recognized that greater fidelity reproduction of the wave contour would be necessary for accurate PWA (17). Despite numerous techniques proposed to enhance the fidelity of reconstructed central waveforms, and devices like the Mobil-O-Graph being clinically available and validated for specific parameters such as central BP and pulse wave velocity, the literature still lacks a robust method and comprehensive analysis of central pressure waveform reconstruction and PWA validated against invasive data (18–22).

To address this unmet need, we incorporated a spectral machine learning algorithm into the brachial cuff system to noninvasively reconstruct the shape of the central pressure waveform. This approach is based on the Fourier decomposition of pressure waveforms and hence is referred to as Fourier-based machine learning

(F-ML). F-ML transforms a peripheral pressure waveform to the central site by applying nonlinear mapping to the fundamental wave components (Fig. 1*B*) (23). This approach is suitable for waveform reconstruction due to its ability to capture high-frequency components in the pressure waveform (24, 25). Our recent work demonstrated the operating principle of F-ML in mapping the radial waveform to the carotid waveform, both acquired using tonometry and calibrated with the same brachial BP (23). While these prior findings provide a proof of concept for the F-ML approach, its clinical applicability and potential as a reliable measurement modality remain unknown. In the present study, the authors aim to reconstruct the central pressure waveform with the F-ML method from an automated brachial cuff system (26) and compare it to an invasive catheter measurement at the ascending aorta (Fig. 1*C*). The measurement modalities of this study—the invasive catheter and the brachial cuff—are entirely independent, enabling a true analysis of the clinical applicability of our approach.

Results

Clinical Characteristics. The study recruited 202 patients referred for nonemergent left heart cardiac catheterization to be performed from either a femoral or radial access site. Manual analysis of the clinical data excluded 44 subjects for failed procedures, leaving a total of 158 subjects in the study; exclusion reasons included 11 catheter malfunctions, 16 cuff malfunctions, 14 incorrect measurement procedures, and three aborted measurements. Upon analysis of the recordings, an additional 33 subjects were excluded for signal degradation (125 subjects remaining), of which 7 were for severe arrhythmia, 11 for sensor saturation, and 15 for poor signal quality. The algorithmic analysis excluded 10 additional subjects, either due to failure in identifying waveform cardinal points or an insufficient number of consecutive waveforms. A total of 115 subjects passed all manual evaluations and algorithmic eligibility criteria to generate a dataset of 3,615 waveforms.

The cohort examined in this investigation (subjects = 115) comprised 63% males, with an average age of 66 y, and a mean Body Mass Index of 28.6 kg/m^2 (*SI Appendix*, Table S1). Subjects had an average left arm circumference of 31 ± 4 cm, with a minimum of 24 cm and a maximum of 42 cm; the used cuff size was appropriate for all subjects in the study. Within the study population, 80% reported hypertension (HTN), 74% reported hyperlipidemia, and 32% reported diabetes mellitus. The study population exhibited a notable prevalence of CVD: 21% reported heart valve disease, 20% reported heart failure, and 19% reported left ventricular dysfunction. Indication for left heart catheterization referral in the examined cohort are summarized in *SI Appendix*, Table S2; the predominant referral reasons included abnormal testing (60%), angina (23%), and diagnostic purposes (15%).

A standard 70:30 train-test split was applied to the study population to generate two independent cohorts: the training cohort for model training (subjects = 80, waveforms = 2,621) and the testing cohort for evaluation (subjects = 35, waveforms = 994). Training and testing cohort characteristics are found in *SI Appendix*, Table S3.

Waveform Reconstruction. Fig. 2*A* shows 10-s segments of the continuous waveform reconstruction from cuff-based F-ML against the true signal measured from the catheter in two sample cases from the testing population. *SI Appendix*, Fig. S2 presents 20-s segments of invasive catheter signals from three test cases in the population, illustrating the pressure fluctuations observed in continuous recordings on a beat-to-beat basis. The SBP tracking precision, shown in Fig. 2*B*, demonstrates a strong linear correlation ($r = 0.76$, $P < 0.05$) between the fluctuation amplitudes measured during breathing cycles by the cuff-based F-ML method and the invasive catheter for subjects in the test population (subjects = 35). Fig. 2*C* shows the Bland–Altman analysis for the SBP fluctuations reporting a bias (B) of 2.4 mmHg with limits of agreement (LOA) of [−6.0, 10.8] mmHg. Waveform reconstruction repeatability in the test population (subjects = 35) was assessed in Fig. 2*D*; the F-ML method had a coefficient of variation (COV) of 0.26 ($MEAN_{avg}$ = 6.9 mmHg; SD_{avg} = 1.8 mmHg). *SI Appendix*, Fig. S3 compares brachial, GTF reconstructed, and F-ML reconstructed continuous waveform signal against the pressure–time signal of the invasive catheter. A comparable COV was reported for GTF (COV = 0.25) but with higher averages for both the RMS error (RMSE) mean ($MEAN_{avg}$ = 8.8 mmHg) and SD (SD_{avg} = 2.2 mmHg) (*SI Appendix*, Fig. S4). A statistically significant difference was found between the mean of RMSE for the GTF and F-ML methods ($P < 0.05$).

Pulse waveforms were further analyzed on a beat-to-beat basis to estimate the reconstruction error for both absolute pressure values and metrics for waveform shape on all waveforms for the test population (subjects = 35, waveforms = 994). Fig. 3*A* shows the error, calculated as true (invasive measurement) minus predicted, for the SBP, DBP, and MAP. The SBP error from the reconstructed waveforms showed a statistically significant difference ($P < 0.05$) between GTF (B [LOA] = 1.7 [−17.6, 21.0] mmHg) and F-ML (B [LOA] = −0.3 [−17.0, 16.4] mmHg). The error in DBP values from the reconstructed waveforms also showed a statistically significant difference ($P < 0.05$) between GTF (B [LOA] = −5.2 [−17.9, 7.4] mmHg) and F-ML (B [LOA] = −0.7 [−13.1, 11.6] mmHg). Table 1 shows a significant improvement in BP measurement for the F-ML method compared to GTF. Notably, the reduction in the bias for DBP contributes to the enhanced correlation for DBP measurement with the F-ML method (R^2 = 0.58, r = 0.76), compared to GTF (R^2 = 0.27, r = 0.77). The lower R^2 for GTF likely reflects the consistent bias in its DBP estimates, despite a similar linear relationship with the catheter measurements.

Shape correspondence between the reconstructed waveform and the true measurement showed statistically significant differences ($P < 0.05$) between GTF and F-ML for the pressure signal, first derivative, and second derivative (Fig. 3*B*). The normalized-RMS error (nRMSE) for the pressure signal reconstruction with F-ML (B [LOA] = 11.3 [1.1, 21.6] %) was lower than that with GTF (B [LOA] = 14.5 [1.2, 27.9] %). *SI Appendix*, Figs. S5–S7 qualitatively show the increased faithfulness of waveform reconstruction with the F-ML method. *SI Appendix*, Fig. S8 presents the F-ML waveform reconstructions alongside their respective aortic catheter waveforms, illustrating examples of waveforms with distinctly different morphologies, as quantified by the augmentation index (AIx) (27). *SI Appendix*, Tables S4 and S5 summarize the shuffle split testing results, showing that the F-ML model's performance is consistent and generalizable across different data splits in the study population.

SBP and DBP from the invasive catheter, F-ML method, and brachial cuff pressure measurement were used to generate HTN classifications for the test population (subjects = 35); the subject-averages for the individual waveform BP values were used in the invasive catheter and F-ML method. Fig. 4 shows the HTN classification results in the form of a confusion matrix for the brachial cuff pressure measurement and F-ML method compared to the gold standard from the invasive aortic catheter. The brachial cuff pressure measurements yielded 12 true negatives, 12 true positives, 11 false positives, and 0 false negatives, with an accuracy of 69%, a sensitivity of 100%, and a specificity of 52% (Fig. 4*A*).

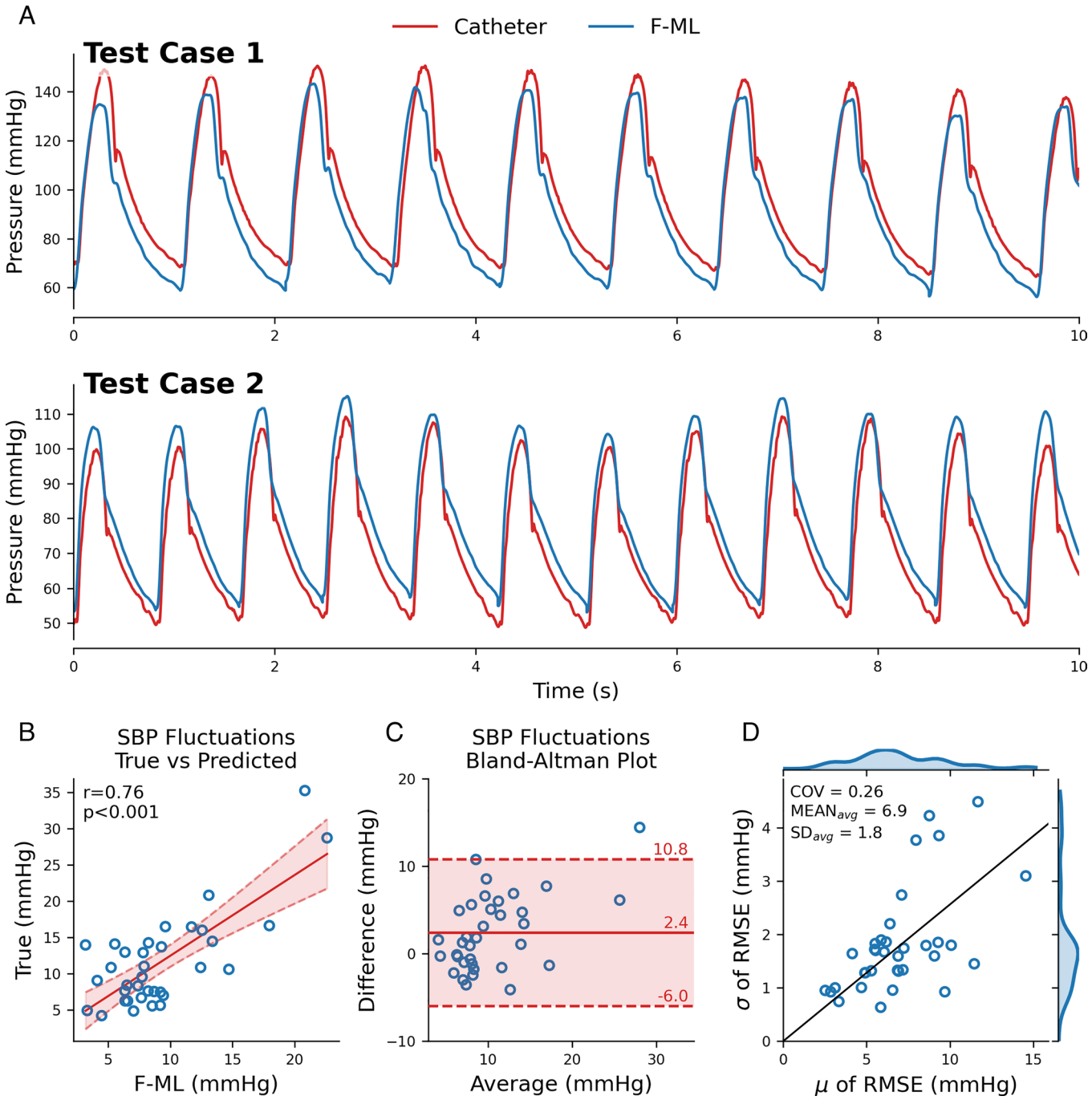

Fig. 2. Evaluation of continuous pulse waveform reconstructions from the F-ML method in the test population (n = 35 subjects). (*A*) Ten-second segments of the invasive catheter signal (red) are compared to the reconstructed continuous F-ML signal (blue) for two test cases. (*B*) True-versus-predicted plot for the subject-averaged peak-to-peak fluctuation amplitude of SBP in mmHg across breathing cycles (n = 35). The red line represents the linear regression line of best fit, with shaded regions indicating the 95% CI for the predictions. The dashed lines show the upper and lower bounds of the CI. (*C*) Bland–Altman plot for the subject-averaged peak-to-peak fluctuation amplitude of SBP in mmHg. The red solid line represents the bias, while the dashed red lines indicate the limits of agreement. (*D*) Subject-level error is quantified as the SD versus the mean RMSE of the continuous pressure signal reconstruction for the F-ML model. The black line represents the coefficient of variation.

The F-ML method showed 18 true negatives, 12 true positives, and 5 false positives and 0 false negatives, with an accuracy of 86%, a sensitivity of 100%, and a specificity of 78% (Fig. 4*B*).

Central Waveform Analysis. Beat-to-beat PWA was performed to extract clinically significant waveform parameters from the true and F-ML reconstructed signals on all cardiac cycles in the test population (subjects = 35, waveforms = 994). Fig. 5 compares clinical parameters derived using PWA from the F-ML reconstructed central waveform (Predicted) with the values obtained from the invasive catheter (True). Area-based parameters are presented in Panel 5A for the systolic pressure time integral (SPTI) (r = 0.91, $P < 0.05$; B [LOA] = 0.2 [−5.6, 6.0] mmHg s), Panel 5B for the diastolic pressure time integral (DPTI) (r = 0.95, $P < 0.05$; B [LOA] = −0.6 [−9.3, 8.0] mmHg s), and Panel 5C for subendocardial viability ratio (SEVR) (r = 0.86, $P < 0.05$; B [LOA] = −0.024 [−0.372, 0.323]). Shape-based parameters are shown in Panel 5D for Form Factor (r = 0.73, $P < 0.05$; B [LOA] = 0.007 [−0.034, 0.048]), Panel 5E for the AIx (r = 0.87, $P < 0.05$; B [LOA] = 1.2 [−19.6, 22.0] %), and Panel 5F for Peak Time (r = 0.80, $P < 0.05$; B [LOA] = 3.5 [−46.5, 53.5] ms).

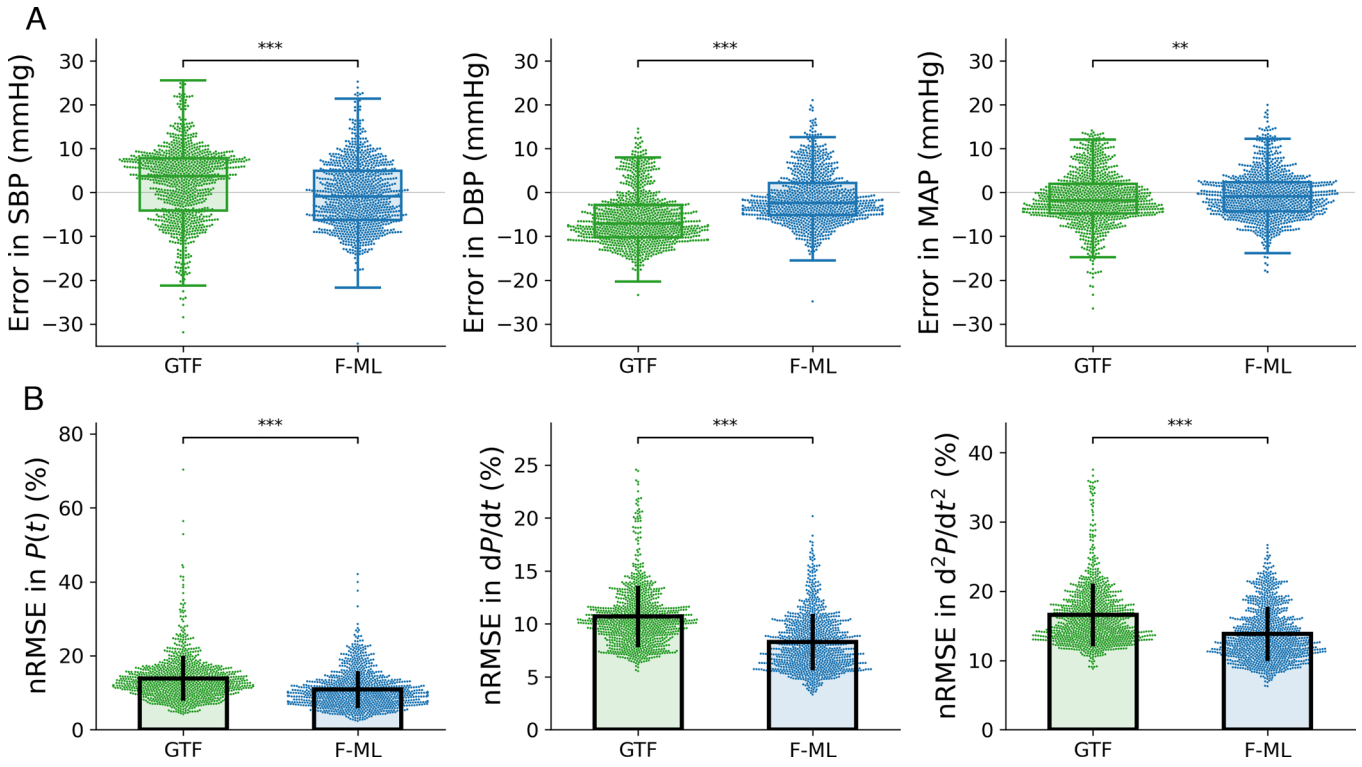

Fig. 3. Beat-to-beat evaluation of GTF and F-ML method predictions compared to the invasive central waveform in the test population (subjects = 35, waveforms = 994). (*A*) Prediction errors (True−Predicted) for SBP, DBP, and MAP are shown for the GTF (green) and F-ML (blue) methods. (*B*) The nRMSE is shown for waveform shapes and their first and second derivatives, comparing the GTF (green) and F-ML (blue) methods. Statistical significance is indicated as $*P < 0.05$, $**P < 0.01$, and $***P < 0.001$.

Pulse waveform parameters related to the timing and location of the dicrotic notch are depicted in Panel 5G for Notch Time (r = 0.82, $P < 0.05$; B [LOA] = 4.1 [−39.3, 47.4] ms) and Panel 5H for Notch Value (r = 0.92, $P < 0.05$; B [LOA] = −0.7 [−14.3, 12.9] mmHg). The analysis for the equivalent parameters measured on the GTF reconstructed waveforms is summarized in *SI Appendix*, Figs. S9 and S10. Further results from the cuff-based F-ML method are reported in *SI Appendix*, Fig. S11 for the slope parameters of maximal pressure rise rate (dP/dt Max) and maximal pressure fall rate (ndP/dt Max) and *SI Appendix*, Fig. S12 for the augmentation pressure (AP) parameter.

The relationship between the subject-averaged values of three pulse waveform parameters—SPTI, DPTI, and SEVR—and age was evaluated for both the catheter measurements and the cuff-based F-ML reconstructions in the test population (subjects = 35) (Fig. 6). Subjects were divided into four age quartiles (Q1 to Q4) to create roughly equal-sized groups: Q1 (subjects = 9, ages 48 to 65), Q2 (subjects = 7, ages 66 to 70), Q3 (subjects = 12, ages 71 to 73), and Q4 (subjects = 7, ages 74 to 82). No statistically significant difference was observed between the true and cuff-based F-ML values for all parameters—SPTI, DPTI, and SEVR—across all age groups. SPTI and DPTI did not show a significant change with age for both the true and F-ML values. SEVR decreased with age for both the true values ($P < 0.05$) and the F-ML values ($P < 0.05$). As a reference, *SI Appendix*, Fig. S13 shows the scatter plots for the SPTI, DPTI, and SEVR parameters from the catheter recording with age for all subjects in the study (subjects = 115).

Discussion

Central BP has been increasingly recognized as a superior predictor of cardiovascular risk and prognostic outcomes compared to peripheral BP (2, 28). Additionally, growing evidence highlights the greater clinical value of central pressure waveform shape, which contains more prognostic information than peripheral waveforms (29–31). This study aimed to develop and validate a method for accurate reconstruction of the central aortic pressure waveform to enable precise PWA. We introduce a machine learning–based approach that leverages nonlinear mapping in the frequency domain to transfer a brachial calibrated waveform into its central aortic counterpart. Unlike traditional methods, our nonlinear mapping accounts for complex wave interactions and distortions that occur as waveforms travel through the cardiovascular system. As demonstrated in Figs. 2 and 3, our method accurately captures central waveform morphology and dynamic fluctuations from a noninvasive brachial measurement—an essential foundation for reliable PWA.

In evaluating the clinical applicability of the proposed approach, we assessed the accuracy of PWA using the F-ML reconstructed waveforms compared to catheter measurements (Fig. 5). This analysis focused on a comprehensive set of clinically relevant parameters that characterize various aspects of the pressure waveform. The area-based features, including SPTI (a measure of myocardial oxygen demand), DPTI (a measure of subendocardial blood supply), and SEVR (a measure of myocardial oxygen supply and demand), demonstrated strong prediction accuracy. Similarly, the shape-based features of Form Factor (the normalized mean of the waveform) and AIx (a measure of wave reflection), and peak time (time to maximal systolic pressure), also exhibited robust predictive performance. Furthermore, parameters characterizing the dicrotic notch, such as Notch Time (a measure of left ventricular ejection duration) and Notch Value (pressure at end-systole), showed strong correlations with the invasive catheter measurements. Lower prediction performance was observed on the slope-based parameters of dP/dt Max and ndP/dt Max (indirect measures of contractility); this is visible in the Bland–Altman plots in *SI Appendix*, Fig. S11 as well as in the first derivative signal in

Table 1. Measurement statistics for central blood pressure predictions using the GTF and F-ML methods compared to catheter values in the test population (subjects = 35, waveforms = 994)

Variables	GTF	F-ML
SBP		
Coefficient of determination (R^2)	0.76	**0.83**
Correlation coefficient (r)	0.89	0.91
RMSE (mmHg)	10.0	8.5
Limit of agreement (mmHg)	38.6	33.4
Mean difference (mmHg)	1.7	−0.3
DBP		
Coefficient of determination (R^2)	0.27	**0.58**
Correlation coefficient (r)	0.77	0.76
RMSE (mmHg)	8.3	6.3
Limit of agreement (mmHg)	25.3	24.6
Mean difference (mmHg)	−5.2	−0.7
MAP		
Coefficient of determination (R^2)	0.67	**0.76**
Correlation coefficient (r)	0.84	0.87
RMSE (mmHg)	6.9	5.9
Limit of agreement (mmHg)	26.7	23.2
Mean difference (mmHg)	−1.3	−0.3

Metrics are calculated using sample weights to ensure equal contribution from all subjects in the test population. Bolded values are used to indicate better performance between the GTF and F-ML methods.

SI Appendix, Figs. S6 and S7. A slight underestimation in the F-ML measurements of the dP/dt Max (11.4% of full variable range) and ndP/dt Max (16.3% of full variable range) was observed. Intrinsically, both parameters reflect the fastest pressure changes within the cardiac cycle, which correspond to the higher frequency components in the waveform's frequency decomposition. Higher frequencies are more susceptible to attenuation during typical smoothing or filtering processes, making them inherently more difficult to predict. As a result, they experience the most significant penalization during the training and prediction phases. Overall, clinical implementation of PWA from the reconstructed central pressure waveform relies on the fidelity of the prediction, and these results are a first step toward this goal.

To fully appreciate the significance of the enhanced reconstructed waveform fidelity from the cuff-based F-ML method, it is worth discussing the underlying mechanisms of this approach and contrasting it with conventional GTF. The GTF method transforms the peripheral waveform to the central waveform through a linear scaling of the Fourier harmonic amplitudes in the frequency space (16, 17). The GTF method was originally reported to be accurate in prediction of the central aortic BP values but required higher fidelity reconstruction for PWA (16, 17). However, this sufficed, as predominantly the central BP values estimated from the noninvasive measurement were used as risk factors for CVD (2). In contrast, the F-ML method employs a support vector regression architecture, utilizing a subset of the frequency content from the peripheral waveform as input to predict each of the central Fourier harmonic amplitudes (23). Both methods operate within the frequency domain, but while the GTF method employs a one-to-one mapping, the F-ML method utilizes a many-to-one mapping, introducing nonlinearities in the response. At a physiological level, the cardiovascular pulse waveform shape is generated by a complex mechanism of forward and reflected propagating waves within the arterial system (32). Therefore, a nonlinear transformation is expected to offer enhanced explanatory power, especially for higher-frequency components, while maintaining generalizability. The high fidelity of F-ML reconstructed aortic pressure waveforms presents an exciting opportunity for future research, such as utilizing the predicted waveforms in mechanistic models to explore the underlying processes driving waveform morphology changes, offering further insight into cardiovascular dynamics. With the increasing applicability of PWA for diagnostic purposes, there has been a growing need for more accurate prediction of the central waveform contour.

While several methods, such as the time-domain model-based approach proposed by Stergiopulos et al. (19) and the adaptive transfer function developed by Gao et al. (18), have been suggested to address the suboptimal fidelity of the reconstructed waveform morphology with GTF, this method remains the standard. Therefore, for our clinical evaluation of the F-ML method, we compared it against GTF. The F-ML approach aligns with current trends in the cardiovascular community, which leverage machine learning for health assessments (33). Our analysis of the predicted central waveforms' pressure–time signal and first derivative corroborates the arguments discussed earlier, demonstrating a significant quantitative improvement in fidelity compared to

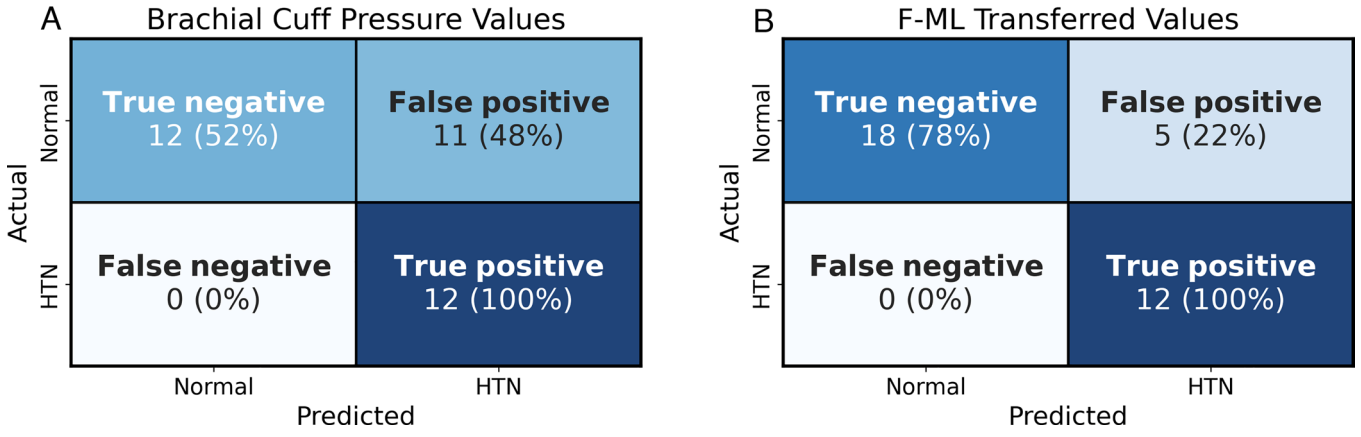

Fig. 4. Comparison of HTN prediction using a confusion matrix for brachial cuff pressure values and F-ML-derived values in the test population (n = 35 subjects). (*A* and *B*) compare the true HTN classification obtained from the invasive catheter in the ascending aorta with the HTN classification values derived from the brachial cuff oscillometric pressure measurement and the F-ML reconstruction of the aortic pressure waveform, respectively. HTN is defined as SBP ≥ 130 mmHg and/or DBP ≥ 80 mmHg.

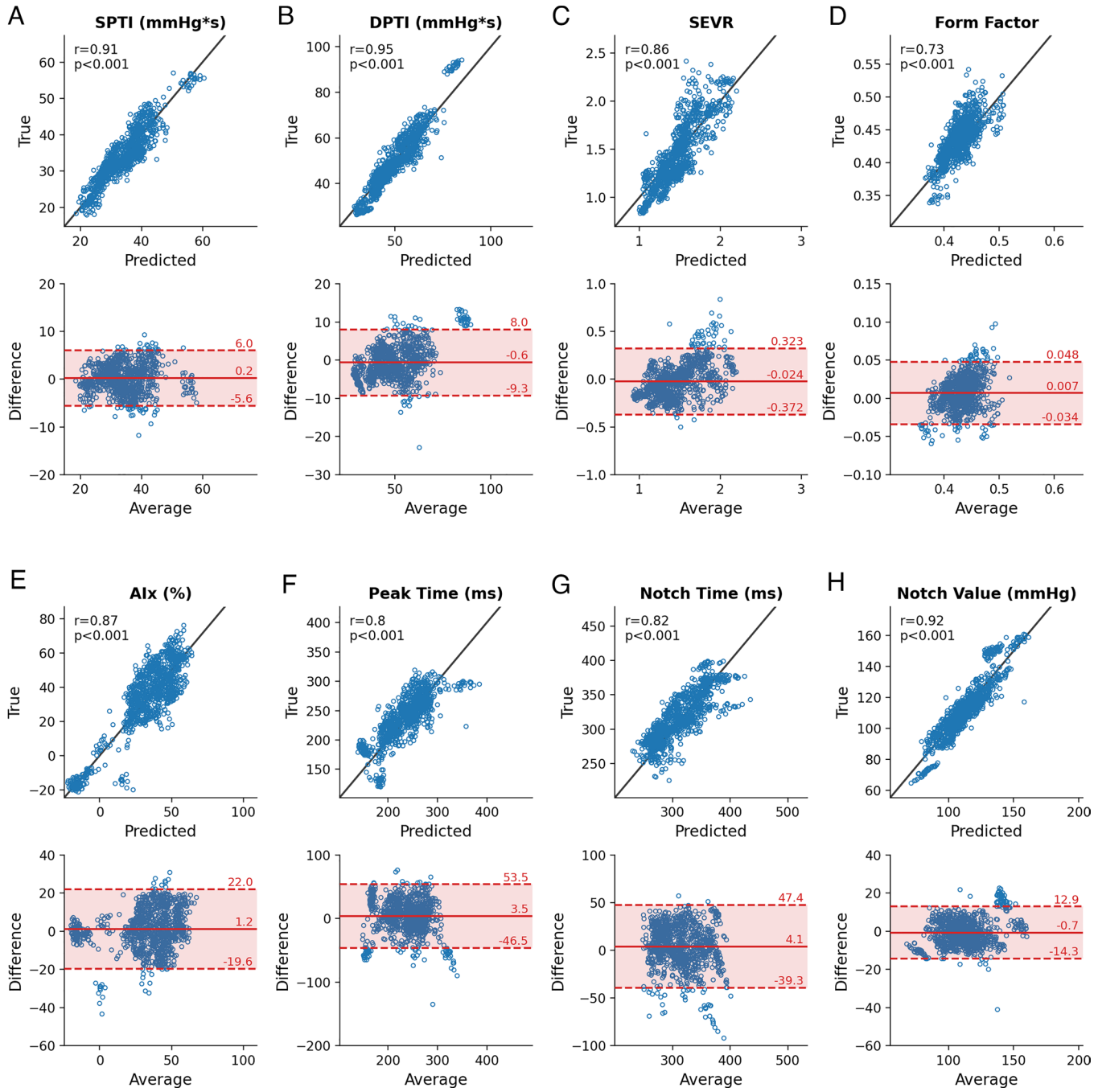

Fig. 5. Assessment of pulse waveform feature prediction accuracy from the F-ML method against the true values from the invasive catheter on individual waveforms in the test population (subjects = 35, waveforms = 994). Prediction accuracy is evaluated using the actual-versus-predicted plots (*Top*) and the Bland–Altman plots (*Bottom*). Eight different features are presented: (*A*) SPTI in mmHg s; (*B*) DPTI in mmHg s; (*C*) SEVR, dimensionless; (*D*) form factor, dimensionless; (*E*) augmentation index (AIX) in %; (*F*) peak time in milliseconds; (*G*) notch time in milliseconds; and (*H*) notch value in mmHg. The Pearson correlation coefficient (r) and corresponding *P*-value are provided for the true-versus-predicted plots. The mean (solid line) and limits of agreement (dashed lines) are shown on the Bland–Altman plots.

its benchmark (Fig. 3 and *SI Appendix*, Figs. S5–S7). The F-ML method places a stronger emphasis on high-frequency components, which are responsible for capturing waveform shape during rapid pressure transitions such as the systolic peak, diastolic dip, and dicrotic notch, all of which hold significant physiological importance. Notably, prediction accuracy enhancements in SBP and DBP were observed with the F-ML method, as these values are directly dependent on the shape of the pressure transitions. Specifically, the F-ML method exhibited a significant prediction improvement for DBP values (Table 1). This advancement is likely attributable to the enhanced prediction of the pressure–time signal around the diastolic dip, which is characterized by a rapid and sudden pressure transition from the opening of the aortic valve. Conversely, MAP shows only moderate improvement as this value is mainly determined by the low-frequency components.

BP values (SBP and DBP) from brachial cuff oscillometric measurements and noninvasively calibrated F-ML waveforms were compared to aortic catheter measurements for HTN classification. The F-ML method demonstrated higher accuracy (86%) compared to the brachial cuff measurements (69%), which is attributable to the lower false positive rate for the F-ML method

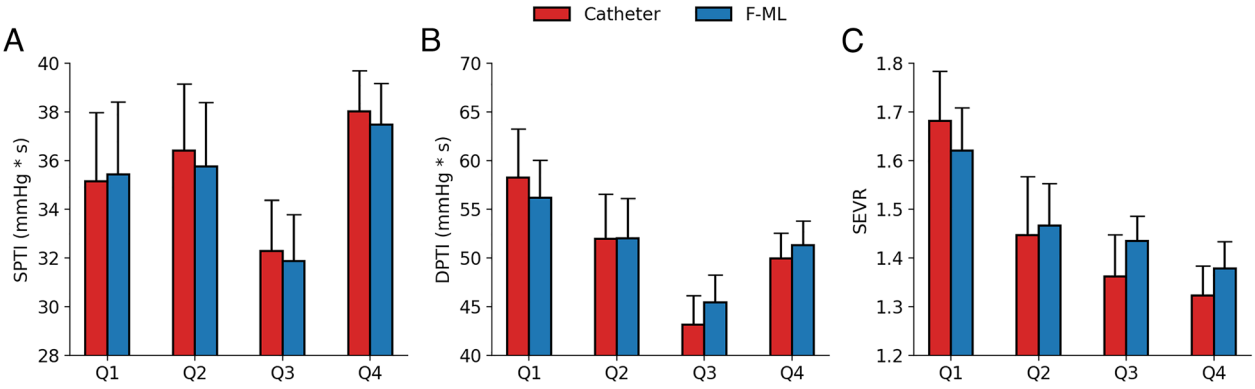

Fig. 6. The SPTI, DPTI, and SEVR as a function of measurement method and age on the test population (n = 35 subjects). (*A*–*C*) show the SPTI, DPTI, and SEVR as a function of age, grouped in quartile ranges, respectively. The red columns are the true values measured using the invasive catheter, and the blue columns are the parameters derived from the cuff with the F-ML method.

(22%) compared to the brachial cuff BP measurements (48%). This difference can be rationalized from pulse pressure amplification—a phenomenon where pressure waves increase in amplitude as they travel from the aorta to the brachial artery, causing patient-specific increases in SBP values (10). By accounting for these central-to-peripheral waveform changes, the F-ML method offers a more accurate assessment of central HTN. While noninvasive calibration methods typically yield less accurate results than invasive techniques, the practical risks associated with invasive measurements pose significant clinical limitations (34). This underscores the importance of advancing fully noninvasive BP estimation methods. By emphasizing higher frequency components and accounting for system nonlinearities, the F-ML method achieves measurable improvements in clinical waveform reconstruction. Furthermore, its adaptability across brachial cuff-based devices, relying only on consistent signal relationships and proper calibration, highlights its broad applicability for noninvasive pressure assessments. Implementing the F-ML method for central PWA in clinical practice requires training the model on paired peripheral (input) and central (output) waveforms to learn the nonlinear mapping between the measurement and target locations. This could follow the approach used in this manuscript, which utilizes a comprehensive dataset of simultaneously measured waveforms. If invasive measurements are unavailable, computational models could be used to generate the target data, allowing the model to be trained with noninvasive (input) measurements (35, 36). Once trained, the F-ML model can then be applied to populations with general characteristics similar to those of the training cohort.

The cuff-based F-ML method was applied to study age-based trends in central pulse waveform parameters, focusing on SPTI, DPTI, and SEVR. Neither SPTI, a measure of myocardial oxygen demand, nor DPTI, a measure of subendocardial blood supply, showed statistically significant age-based trends. However, SEVR, a measure of myocardial oxygen supply and demand, decreased with age for both the true catheter values and the cuff-based F-ML values, with statistically significant results ($P < 0.05$). These findings are consistent with existing literature indicating a decline in SEVR with age (37, 38). Hayward et al. (39) also observed a gender-specific decrease in SEVR with age, noting this trend exclusively among women. SEVR is an important cardiac metric associated with increased cardiovascular disease risk and can be used to assess coronary microcirculation in essential hypertensives (38, 40, 41). This invasive study further confirms the age-related decrease in the SEVR, as measured invasively with a catheter in the ascending aorta, and highlights the ability to noninvasively measure this index using a brachial cuff.

The study's major limitation is the exclusive recruitment of subjects referred for left heart catheterization, which may introduce a selection bias. The population exhibits a prevalence of severe cardiovascular conditions, advanced age with limited variability, and a high burden of comorbidities. Consequently, this sample is not representative of the general population, potentially limiting the applicability of these specific results. However, this concern is mitigated by the previous validation of the F-ML method on a large heterogenous cohort (23). Furthermore, the robust outcomes observed within this highly diseased population are encouraging, as these cases typically represent more complex scenarios. Future studies should aim to explore the applicability of cuff-based F-ML among diseased populations, addressing the question of whether a single model can adequately generalize across different conditions and cohorts.

In this invasive study, we showed that the cuff-based F-ML approach is an accurate and precise method for central hemodynamic assessment from a peripheral measurement site with noninvasive calibration. The developed method successfully reconstructed both individual waveforms and the continuous pressure–time signal, capturing magnitude and breathing-induced BP fluctuations, as measured with an invasive aortic catheter. Application of PWA to the central waveforms reconstructed with cuff-based F-ML extracted clinical parameters that showed strong agreement with those measured from the invasive catheter. Furthermore, population-wide trends in SPTI, DPTI, and SEVR parameters showed consistent age-dependent behaviors between the cuff-based F-ML and catheter measurements; in particular, the SEVR parameter which is indicative of the subendocardial oxygen supply–demand ratio decreased with age. Overall, our results demonstrate the feasibility of aortic pressure waveform reconstruction through the cuff-based F-ML approach with noninvasive calibration and its applicability in providing an accurate noninvasive assessment of central hemodynamics.

Materials and Methods

Study Design. This study recruited subjects scheduled for cardiac catheterization between September 2021 and September 2022. The main inclusion criteria included age greater than 21 y, referral for nonemergent left heart catheterization, and ability to participate in all study evaluations. Study exclusion criteria included occurrence of a severe cardiac event within a week of catheterization, inability to obtain a brachial BP measurement, and contraindication to cardiac

catheterization by judgment of the interventional cardiologist. The protocol and analysis were conducted in accordance with the guidelines outlined by Sharman et al. (42) for validating noninvasive central BP devices. This cross-sectional study followed the STROBE statement guidelines, a completed checklist is reported in *SI Appendix*, Fig. S1.

The study was approved by Western and Salus International Review Boards. Participants provided written informed consent before the procedure. The study was conducted in accordance with the principles outlined in the Declaration of Helsinki. The following health centers participated in the study: Princeton Baptist, AL; LSU Health Sciences Center, CA; Long Beach Memorial Care Hospital System, CA; Orange Coast Memorial Care Hospital, CA; and Saddleback Memorial Care Hospital System, CA.

Study Devices. The study consisted of simultaneous recordings of invasive aortic catheterizations and noninvasive pulse waveform acquisition with brachial cuff devices. The study necessitated cuff placement on the subject's left arm in accordance with standard cuff-placement guidelines. Cardiac catheterization was conducted using either femoral or radial access; for the radial artery, catheter access was limited to the right radial site. To minimize potential hydrostatic pressure differences between these independent measurement modalities, simultaneous measurements were performed in the supine position, with the left arm positioned adjacent to mid-chest height.

This study utilized the Millar Mikro-Cath pressure catheter, a single-use, solid-state device. The catheter was zeroed before insertion at the access sites, and the accuracy of the zeroing was manually confirmed in the recorded signal prior to analysis. Solid-state catheters are less sensitive to positional changes, reducing the influence of hydrostatic pressure variations. In the measurement range from −50 to 300 mmHg, the Mikro-Cath has a reported accuracy of ±1% of reading from −50 to 50 mmHg and ±3% of reading from 50 to 300 mmHg. The brachial cuff device used in this study is an investigational device for high-resolution noninvasive pulse waveform acquisition developed and validated by Tamborini and Gharib (26, 43–45). The apparatus consisted of a noninvasive BP module (NIBP 2020 UP) equipped with oscillometric BP capabilities and tourniquet mode, complemented by a custom pneumatic system designed for pulse waveform capture. The system uses a cuff designed for arm circumferences from 22 cm to 42 cm. The device was configured to execute a BP measurement used for calibration purposes followed by tourniquet mode using the inflate-and-hold approach. By default, the oscillometric BP measurement is configured in inflation mode, and resorts to a deflation-based measurement only upon measurement failure. Pulse waveform acquisition using the inflate-and-hold approach was conducted at the suprasystolic pressure (sSBP), defined as the SBP plus an additional 35 mmHg. The sSBP level ensures that the cuff remains above the systolic threshold, fully occluding arterial flow, and has been shown to closely represent the true pressure waveform (26). The waveform measurement was conducted for a duration of 40 s. The full measurement had an approximate start-to-end duration of 140 s. The oscillometric pressure measurement has a manufacturer-reported accuracy of ± 3 mmHg or 2%, whichever is greater, within the operating range, and has a pressure transducer accuracy of ± 1 mmHg. Data were acquired at a sampling rate of 1 kHz.

Noninvasively captured brachial pressure waveforms accurately represent the true pressure waveform shape but are measured in nonphysiological units (i.e., uncalibrated). Calibration is then performed to scale the waveforms to true physiological values, reflecting SBP and DBP. Calibration of the noninvasive waveforms was performed using noninvasive BP values from the brachial cuff oscillometric measurements, as commonly used in routine clinical practice. The SBP and DBP values from the brachial cuff oscillometric reading are corrected using previously validated relationships and applied to define the peak (SBP) and base (DBP) of each cardiac cycle (26). BP fluctuations were introduced using the envelope function dynamic calibration method, which was previously described and validated by Tamborini and Gharib (26). This method exploits the patient-specific envelope function, which relates the pulse amplitude in the cuff to the nominal cuff pressure typically used for oscillometric measurement. The pressure fluctuation is measured by the deviation of the current cardiac cycle's cuff pressure amplitude at a nominal cuff pressure from the established envelope function. The SBP and DBP values from the cuff are then adjusted for each cardiac cycle to reflect breathing-induced pressure fluctuations.

Data Preprocessing. Data quality control was applied to exclude measurements affected by cuff or catheter malfunction, measurement errors, signal saturation, irregular heart rate, poor signal quality, or algorithmic failures. This process involved a detailed inspection of the raw data from both modalities. For the catheter, proper zeroing was ensured to minimize hydrostatic effects, and measurements with positioning discrepancies or drift were excluded. For the cuff, special attention was given to identifying inconsistencies in the oscillometric technique, such as movement artifacts or improper placement. Additionally, both modalities were checked for signal distortion, particularly during large pressure variations, and measurements from patients with irregular heart rates or unstable hemodynamics were flagged and excluded to prevent misrepresentation.

Simultaneous aortic catheter and brachial cuff pressure recordings were preprocessed for model training and testing. Pressure–time waveforms were segmented into cardiac cycles, indexed from the foot of the waveform, defined as the local minimum preceding the systolic pressure rise. Cardiac cycles were retained only if they met validity criteria, including appropriate signal length, accurate indexing of all cardinal points (e.g., foot, peak, and dicrotic notch), and correct placement of these indexes by the algorithm. Only cardiac cycles satisfying these criteria for both aortic and brachial waveforms were included and appended to a shared dataframe. Valid cycles were transformed to the frequency domain using the Fast Fourier Transform (FFT), with only the first 20 Fourier modes retained for analysis. Features were normalized to the [0,1] range with parameters fitted on the training set and applied to the testing set. Noisy or incomplete data were excluded to ensure high-quality inputs for modeling.

F-ML Method. The F-ML method is a well-established method to transfer the peripheral pressure waveform to the central site and its working principle has been shown in a large heterogeneous population cohort (23). The F-ML method implemented in this study uses Support Vector Regression for the reconstruction of the central pressure waveform (46). The model input are the first 20 modes from the Fourier decomposition of the peripheral pressure waveform; the model output are the first 20 modes of the estimated central pressure waveform. It has been shown the first 20 modes are sufficient to fully reconstruct the cardiovascular pulse waveform (23). Central waveform reconstruction involves applying the inverse Fourier transform to the predicted modes and adjusting for the length of the cardiac cycle. Model fitting is strictly performed on the training set, and model evaluation is exclusively performed on the testing set. Further details regarding the method are in *SI Appendix*, *Supporting Text* 1. Validation of the F-ML method was performed using the invasive aortic catheter pressure recording as the gold standard.

Improvements of the F-ML method were evaluated in comparison to the conventional method for central pressure waveform reconstruction from peripheral measurements, the GTF method (16, 17). The GTF for this study population is computed on a weighted average of the individual transfer functions obtained from each pair of central and brachial pulse waveforms from the training samples. The weighing is computed to ensure each subject gives the same contribution in the GTF, irrespective of the number of cardiac cycles in the dataset. Individualized transfer functions are computed over bins of size 1 Hz. Evaluation is performed on the testing samples.

Continuous pressure time signal reconstructions of the central aortic waveforms, for both the F-ML and GTF methods, were generated by sequentially processing and concatenating individual cardiac cycles in the time domain. To predict the continuous signal for a set number of waveforms, the Fourier modes for each individual waveform were provided as separate inputs. The methods predicted the output modes for each waveform independently, which were then transformed into the time domain and concatenated sequentially to reconstruct the continuous pressure waveform.

Statistical Analyses. Data splitting for training and testing is performed at the subject level such that no cardiac cycles from a subject are in both sets. A 70% train and 30% test size are used. Within these sets, all individuals had at least five consecutive valid simultaneous cuff and catheter cardiac cycles. Method evaluation was performed for each subject on the continuous pressure–time signal reconstruction as well as the individual cardiac cycle level. The analysis of the reconstructed continuous pressure–time signal involved two assessments: the average amplitude of SBP fluctuations during the breathing cycle and the RMSE of the waveform across the sSBP recording. For each participant, the average

and SD of the RMSE were juxtaposed to investigate the correlation between the variability of errors and their magnitudes, as represented by the COV.

We evaluated the accuracy of F-ML and GTF in estimating SBP, DBP, and MAP. SBP was defined as the peak pressure of the waveform, DBP as the minimum pressure in diastole, and MAP as the average pressure of the waveform. Our analysis compared BP values derived from F-ML and GTF for individual cardiac cycles with those invasively measured using a catheter in the ascending aorta of the simultaneous cardiac cycle. Evaluation metrics included the Pearson correlation coefficient (r) to measure the degree of linear association, the coefficient of determination (R^2) to assess the prediction accuracy against true values, the RMSE to quantify the error, the bias with limits of agreement; all metrics were weight-adjusted to give equal importance to all subjects regardless of number of cardiac cycles. Brachial cuff oscillometric measurement values, F-ML derived values, and catheter values of subject-averaged SBP and DBP were used to identify cases of HTN using the guidelines reference values (SBP ≥ 130 and/or DBP ≥ 80) (47). Classification analysis for HTN included accuracy, sensitivity, and specificity.

We evaluated the morphological reconstruction error of F-ML and GTF waveforms for the pressure–time signal and its first and second derivatives. Evaluation was performed using nRMSE across the cardiac cycle, where normalization was applied by the pulse pressure amplitude of the true signal. Reconstructed waveforms were compared against invasive waveforms measured with a catheter in the ascending aorta during the same cardiac cycle. Signal derivatives were calculated using discrete differentiation and Savitzky–Golay filtering. A shuffle split analysis with 15 subject-level splits was performed on the entire study population to evaluate the consistency and generalizability of the F-ML methodology. The model was retrained for each split, and the predicted waveforms were assessed for accuracy in both waveform morphology and BP values prediction.

PWA was applied to individual cardiac cycles to extract clinically significant features that perform a comprehensive characterization of the pressure waveform. This analysis included the extraction of area-based features, shape-based features, dicrotic notch parameters, and slope-based features. Area-based features comprised the SPTI (48), DPTI (48), and SEVR (48). Shape-based features included the form factor (49), AIx (50), AP (50), and peak timing (51). Dicrotic notch parameters were used to assess the timing and pressure magnitude of the notch; notch timing was determined using the index of maximal negative pressure derivative (52), while the notch value was defined as the pressure value at the time instance. Finally, slope-based parameters included dP/dt Max (53), and ndP/dt Max (53). Pulse waveform feature agreement and bias were assessed by comparing the predicted values to the true values obtained from the invasive catheter measurement, using true-versus-predicted plots and Bland–Altman analysis. Results are reported as the Pearson Correlation Coefficient (r) and the bias with limits of agreement (B [LOA]) calculated on the individual waveforms in the test population. Statistically significant differences between groups were evaluated using the nonparametric Mann–Whitney *U* test. Two-tailed $P < 0.05$ were considered statistically significant. All analysis performed on the clinical data uses codes written in Python 3.7.

Data, Materials, and Software Availability. Data were obtained from a data transfer and use agreement between Caltech and Avicena LLC (d.b.a. Ventric Health). Further inquiries to https://www.ventrichealth.com/ (54). Code is publicly available (https://github.com/alessiotamborini/FML-TransferFunction) (46).

Author affiliations: [a]Department of Medical Engineering, California Institute of Technology, Pasadena, CA 91125

1. S. S. Martin *et al.*, 2024 heart disease and stroke statistics: A report of US and Global data from the American Heart Association. *Circulation* **149**, e347–e913 (2024).
2. M. J. Roman *et al.*, Central pressure more strongly relates to vascular disease and outcome than does brachial pressure: The Strong Heart Study. *Hypertension* **50**, 197–203 (2007).
3. D. Terentes-Printzios, V. Gardikioti, C. Vlachopoulos, Central over peripheral blood pressure: An emerging issue in hypertension research. *Heart Lung Circ.* **30**, 1667–1674 (2021).
4. J. A. Chirinos *et al.*, Aortic pressure augmentation predicts adverse cardiovascular events in patients with established coronary artery disease. *Hypertension* **45**, 980–985 (2005).
5. C. Vlachopoulos *et al.*, Prediction of cardiovascular events and all-cause mortality with central haemodynamics: A systematic review and meta-analysis. *Eur. Heart J.* **31**, 1865–1871 (2010).
6. L. L. Cooper *et al.*, Intrinsic frequencies of carotid pressure waveforms predict heart failure events: The Framingham Heart Study. *Hypertension* **77**, 338–346 (2021).
7. E. J. Kroeker, E. H. Wood, Comparison of simultaneously recorded central and peripheral arterial pressure pulses during rest, exercise and tilted position in man. *Circulat. Res.* **3**, 623–632 (1955).
8. P. Segers *et al.*, Amplification of the pressure pulse in the upper limb in healthy, middle-aged men and women. *Hypertension* **54**, 414–420 (2009).
9. A. Aghilinejad, F. Amlani, S. P. Mazandarani, K. S. King, N. M. Pahlevan, Mechanistic insights on age-related changes in heart-aorta-brain hemodynamic coupling using a pulse wave model of the entire circulatory system. *Am. J. Physiol. Heart Circulat. Physiol.* **325**, H1193–H1209 (2023).
10. A. P. Avolio *et al.*, Role of pulse pressure amplification in arterial hypertension. *Hypertension* **54**, 375–383 (2009).
11. L. B. Rowell, G. L. Brengelmann, J. R. Blackmon, R. A. Bruge, J. A. Murray, Disparities between aortic and peripheral pulse pressures induced by upright exercise and vasomotor changes in man. *Circulation* **37**, 954–964 (1968).
12. C. M. McEniery, J. R. Cockcroft, M. J. Roman, S. S. Franklin, I. B. Wilkinson, Central blood pressure: Current evidence and clinical importance. *Eur. Heart J.* **35**, 1719–1725 (2014).
13. A. Kollias, S. Lagou, M. E. Zeniodi, N. Boubouchairopoulou, G. S. Stergiou, Association of central versus brachial blood pressure with target-organ damage. *Hypertension* **67**, 183–190 (2016).
14. B. Williams *et al.*; CAFE Investigators; Anglo-Scandinavian Cardiac Outcomes Trial Investigators; CAFE Steering Committee and Writing Committee, Differential impact of blood pressure-lowering drugs on central aortic pressure and clinical outcomes. *Circulation* **113**, 1213–1225 (2006).
15. T. Sharir *et al.*, Validation of a method for noninvasive measurement of central arterial pressure. *Hypertension* **21**, 74–82 (1993).
16. M. Karamanoglu, M. F. O'Rourke, A. P. Avolio, R. P. Kelly, An analysis of the relationship between central aortic and peripheral upper limb pressure waves in man. *Eur. Heart J.* **14**, 160–167 (1993).
17. C.-H. Chen *et al.*, Estimation of central aortic pressure waveform by mathematical transformation of radial tonometry pressure. *Circulation* **95**, 1827–1836 (1997).
18. M. Gao *et al.*, A simple adaptive transfer function for deriving the central blood pressure waveform from a radial blood pressure waveform. *Sci. Rep.* **6**, 33230 (2016).
19. N. Stergiopulos, B. E. Westerhof, N. Westerhof, Physical basis of pressure transfer from periphery to aorta: A model-based study. *Am. J. Physiol.* **274**, H1386–H1392 (1998), 10.1152/ajpheart.1998.274.4.H1386.
20. A. M. Patel, J. K.-J. Li, B. Finegan, M. S. McMurtry, Aortic pressure estimation using blind identification approach on single input multiple output nonlinear wiener systems. *IEEE Trans. Biomed. Eng.* **65**, 1193–1200 (2018).
21. D. Benas *et al.*, Pulse wave analysis using the Mobil-O-Graph, Arteriograph and Complior device: A comparative study. *Blood Press.* 28, 107–113 (2019).
22. W. Weiss *et al.*, Oscillometric estimation of central blood pressure: Validation of the Mobil-O-Graph in comparison with the SphygmoCor device. *Blood Press. Monit.* **17**, 128 (2012).
23. A. Aghilinejad, A. Tamborini, M. Gharib, A new methodology for determining the central pressure waveform from peripheral measurement using Fourier-based machine learning. *Artif. Intell. Med.* **154**, 102918 (2024), 10.1016/j.artmed.2024.102918.
24. A. Aghilinejad, M. Gharib, Assessing pressure wave components for aortic stiffness monitoring through spectral regression learning. *Eur. Heart J. Open* **4**, oeae040 (2024).
25. A. Aghilinejad, A. Tamborini, M. Gharib, Abstract 4142004: Predicting cardiovascular disease events using uncalibrated non-invasive carotid pressure wave components from spectral regression learning. *Circulation* **150**, A4142004–A4142004 (2024).
26. A. Tamborini, M. Gharib, Validation of a suprasystolic cuff system for static and dynamic representation of the central pressure waveform. *J. Am. Heart Assoc.* **13**, e033290 (2024).
27. J. P. Murgo, N. Westerhof, J. P. Giolma, S. A. Altobelli, Aortic input impedance in normal man: Relationship to pressure wave forms. *Circulation* **62**, 105–116 (1980).
28. S. Yu *et al.*, Central Blood Pressure predicts the future cardiovascular risk better than peripheral Blood Pressure: The northern shanghai study. *Eur. Heart J.* **44**, ehad655.2334 (2023).
29. B. Pannier, A. P. Guérin, S. J. Marchais, M. E. Safar, G. M. London, Stiffness of capacitive and conduit arteries. *Hypertension* **45**, 592–596 (2005).
30. P. S. Saba *et al.*, Relation of arterial pressure waveform to left ventricular and carotid anatomy in normotensive subjects. *J. Am. Coll. Cardiol.* **22**, 1873–1880 (1993).
31. I. B. Wilkinson *et al.*, Changes in the derived central pressure waveform and pulse pressure in response to angiotensin II and noradrenaline in man. *J. Physiol.* **530**, 541–550 (2001).
32. L. L. Cooper *et al.*, Components of hemodynamic load and cardiovascular events. *Circulation* **131**, 354–361 (2015).
33. G. F. Mitchell *et al.*, Vascular age assessed from an uncalibrated, noninvasive pressure waveform by using a deep learning approach: The AI-vascularAge model. *Hypertension* **81**, 193–201 (2024).
34. S. A. Hope, I. T. Meredith, J. D. Cameron, Effect of non-invasive calibration of radial waveforms on error in transfer-function-derived central aortic waveform characteristics. *Clin. Sci.* **107**, 205–211 (2004).
35. P. Reymond, F. Merenda, F. Perren, D. Rüfenacht, N. Stergiopulos, Validation of a one-dimensional model of the systemic arterial tree. *Am. J. Physiol. Heart Circ. Physiol.* **297**, H208–H222 (2009).
36. S. Pagoulatou, D. Adamopoulos, G. Rovas, V. Bikia, N. Stergiopulos, The effect of left ventricular contractility on arterial hemodynamics: A model-based investigation. *PLoS One* **16**, e0255561 (2021).
37. N. A. Carlini, R. M. T. Cloud, M. P. Harber, B. S. Fleenor, Cardiorespiratory fitness is associated with estimates of myocardial perfusion: Influence of age and sex. *Am. J. Physiol. Heart Circ. Physiol.* **326**, H103–H109 (2024).
38. V. Aursulesei Onofrei *et al.*, Subendocardial viability ratio predictive value for cardiovascular risk in hypertensive patients. *Medicina (Kaunas)* **59**, 24 (2022).
39. C. S. Hayward, R. P. Kelly, Gender-related differences in the central arterial pressure waveform. *J. Am. Coll. Cardiol.* **30**, 1863–1871 (1997).
40. E. Laugesen *et al.*, Reduced subendocardial viability ratio is associated with unfavorable cardiovascular risk profile in women with short duration of type 2 diabetes. *Am. J. Hypertens.* **29**, 1165–1172 (2016).
41. D. Tsiachris *et al.*, Subendocardial viability ratio as an index of impaired coronary flow reserve in hypertensives without significant coronary artery stenoses. *J. Hum. Hypertens.* **26**, 64–70 (2012).

42. J. E. Sharman *et al.*, Validation of non-invasive central blood pressure devices: ARTERY Society task force consensus statement on protocol standardization. *Eur. Heart J.* **38**, 2805–2812 (2017).
43. A. Tamborini, M. Gharib, A pneumatic low-pass filter for high-fidelity cuff-based pulse waveform acquisition. *Ann. Biomed. Eng.* **51**, 2617–2628 (2023).
44. A. Tamborini, M. Gharib, Listening to heart sounds through the pressure waveform. *Sci. Rep.* **14**, 26824 (2024).
45. A. Tamborini, A. Aghilinejad, M. Gharib, Abstract 4141635: Reconstructing invasive aortic pressure waveforms from non-invasive brachial measurements using a machine learning approach. *Circulation* **150**, A4141635–A4141635 (2024).
46. A. Tamborini, A. Aghilinejad, M. Gharib, F-ML transfer function. GitHub. https://github.com/alessiotamborini/FML-TransferFunction. Deposited 11 December 2024.
47. P. K. Whelton *et al.*, 2017 ACC/AHA/AAPA/ABC/ACPM/AGS/APhA/ASH/ASPC/NMA/PCNA guideline for the prevention, detection, evaluation, and management of high blood pressure in adults: A Report of the American College of Cardiology/American Heart Association task force on clinical practice guidelines. *Hypertension* **71**, e13–e115 (2018).
48. G. D. Buckberg, D. E. Fixler, J. P. Archie, J. I. Hoffman, Experimental subendocardial ischemia in dogs with normal coronary arteries. *Circ. Res.* **30**, 67–81 (1972).
49. R. Alavi *et al.*, A coupled atrioventricular–aortic setup for in-vitro hemodynamic study of the systemic circulation: Design, fabrication, and physiological relevancy. *PLoS One* **17**, e0267765 (2022).
50. J. E. Sharman, J. E. Davies, C. Jenkins, T. H. Marwick, Augmentation index, left ventricular contractility, and wave reflection. *Hypertension* **54**, 1099–1105 (2009).
51. T. Maruhashi *et al.*, Upstroke time is a useful vascular marker for detecting patients with coronary artery disease among subjects with normal ankle-brachial index. *J. Am. Heart Assoc.* **9**, e017139 (2020).
52. P. S. Nandi, D. H. Spodick, Determination of systolic intervals utilizing the carotid first derivative. *Am. Heart J.* **86**, 495–500 (1973).
53. A. H. Khan, D. H. Spodick, The first derivative of the carotid displacement pulse. *Am. Heart J.* **84**, 470–477 (1972).
54. Ventric Health. https://www.ventrichealth.com/. Accessed 16 November 2022.